Improved scintillation time response in (Lu0.5Gd0.5)2O3:Eu3+ compared with Lu2O3:Eu3+ transparent ceramics

Hélène Rétot, Samuel Blahuta, Aurélie Bessière, Bruno Viana, Brian Lacourse, Eric Mattmann

Improved scintillation time response in $(Lu_{0.5}Gd_{0.5})_2O_3 : Eu^{3+}$ compared to $Lu_2O_3 : Eu^{3+}$ transparent ceramics

Hélène Rétot [1,2], *Samuel Blahuta* [1,2], *Aurélie Bessière* [1]*, *Bruno Viana* [1]

Brian LaCourse [2], *Eric Mattmann* [2]

[1] Laboratoire de Chimie de la Matière Condensée de Paris, UMR - CNRS 7574, Chimie-Paristech, 11 rue Pierre et Marie Curie, 75231 Paris Cedex 05, France.

[2] Saint-Gobain Cristaux et Détecteurs, 104 Route de Larchant, 77140 St Pierre les Nemours, France

* tel number : +33 1 53 73 79 43 / fax number : +33 1 46 34 74 89 / e-mail : aurelie-bessiere@chimie-paristech.fr

Abstract

The scintillation properties of two sesquioxides ceramics $Lu_2O_3:Eu^{3+}$ and $(Lu_{0.5}Gd_{0.5})_2O_3:Eu^{3+}$ were studied. Both ceramics present comparable transparency and light yield whereas $(Lu_{0.5}Gd_{0.5})_2O_3:Eu^{3+}$ showed an order of magnitude reduced afterglow in the 3-300 ms range. A thorough study of the location and behavior of Eu^{3+} dopant ions at C_2 and S_6 sites of Lu_2O_3 and $(Lu_{0.5}Gd_{0.5})_2O_3$ structures was carried out with low temperature selective excitation of Eu^{3+}. This revealed that (i) at both C_2 and S_6 sites, Eu^{3+} 4f-4f lifetime is shorter in $(Lu_{0.5}Gd_{0.5})_2O_3:Eu^{3+}$ than in $Lu_2O_3:Eu^{3+}$ (ii) the host matrix $(Lu_{0.5}Gd_{0.5})_2O_3$ as compared to Lu_2O_3 favors the location of Eu^{3+} at C_2 site. As decay times of Eu^{3+} in C_2 and S_6 sites are 1.0 ms and 3.8 ms respectively, the preferred occupation of C_2 in $(Lu_{0.5}Gd_{0.5})_2O_3:Eu^{3+}$ implies a much shorter decay time for $(Lu_{0.5}Gd_{0.5})_2O_3:Eu^{3+}$ in the 3-20 ms range. Reduction of afterglow in the 20-300 ms range is illustrated by thermally stimulated luminescence peaks presenting a highly reduced intensity for $(Lu_{0.5}Gd_{0.5})_2O_3:Eu^{3+}$ compared to $Lu_2O_3:Eu^{3+}$ implying reduced charge trapping defects in $(Lu_{0.5}Gd_{0.5})_2O_3:Eu^{3+}$ ceramics.

Keywords: ceramics, scintillation, Computed Tomography, luminescence, sesquioxide

Introduction

A scintillator is a material able to detect ionizing radiation (X, α, β, γ-rays, neutrons...) and convert them into visible light. In order to obtain performant scintillators the high energy electron-hole pairs produced after ionisation should be efficiently transferred to the luminescent center. This last stage is very material-dependent. One of the most important application fields of scintillation is medical imaging. Today the main scintillating materials for medical imaging are Gd_2O_2S:Pr,Ce,F [1], (Y,Gd)O_3:Eu,Pr [2] and $CdWO_4$ [3,4] for X-ray Computed Tomography (CT) whereas BGO ($Bi_4Ge_3O_{12}$) [5,6], NaI:Tl [7], LYSO ((Lu,Y)SiO_5:Ce^{3+}) [8,9] and LPS ($Lu_2Si_2O_7$) [10,11,12] are often used for Positron Emission Tomography (PET). BGO [13], LYSO [14] and CsI:Tl [13] have also been shown useful for megavoltage X-Ray imaging (portal imaging and cone-beam CT). In the aim of decreasing the radiation dose received by the patient during a scan, scintillators with enhanced efficiency are being investigated. In the first stage of detection, the ionizing radiation must be stopped by the scintillator within the shortest range of the material in order to produce sharp images. High density and high effective atomic number are required for the host material. In that respect lutetium sesquioxide Lu_2O_3 constitutes one of the best possible hosts with a density ρ of 9.43 g/cm^3 and an effective atomic number Z_{eff} of 69. With its cubic structure it can be synthesized as a transparent ceramics which is very advantageous to produce scintillators at a lower cost. However obtaining a nanosecond fast response in Lu_2O_3 from 5d-4f emissions of dopants such as Ce^{3+}, Pr^{3+} or Tb^{3+} was found impossible due to the location of the 5d levels of Ln^{3+} (Ln = Ce, Pr, Tb) inside the conduction band [15]. Nevertheless Eu^{3+} 4f-4f luminescence is observed in Lu_2O_3:Eu^{3+}. It presents a

typical red luminescence that matches very well the sensitivity spectrum of photodiode detectors and its decay time is in the order of millisecond in most hosts [16]. Lempicki *et al.* in 2002 were the first to claim the use of $Lu_2O_3:Eu^{3+}$ ceramics as a scintillator [17]. While a typical 1-2 ms response time is considered as totally acceptable for scintillators in X-rays CT application, longer afterglow should be suppressed so that CT images do not get blurred by delayed signals. Unfortunately afterglow is often a limiting parameter in sesquioxide hosts. An afterglow of some hundreds of milliseconds has been reported by several authors in $Lu_2O_3:Eu^{3+}$ [18,19,20] as well as in $Lu_2O_3:Tb^{3+}$ [21]. The afterglow in sesquioxides could originate from Frenkel defects as the structure allows easy displacement of oxygen atoms. However no experimental proof has been brought up till now. Alternatively co-doping was reported as a way to reduce afterglow in some cases. Pr^{3+} [22] or Ti^{4+} [23] co-doping in $(Y,Gd)_2O_3:Eu^{3+}$ for instance were found to reduce persistent luminescence of Eu^{3+}. On the contrary Ca^{2+} addition in Lu_2O_3: Tb^{3+} [21] enhanced long-lasting luminescence in the material.

In this work an alternate way to improve time response in Eu^{3+}-doped sesquioxides is reported. By heavily substituting the lutetium host cation with gadolinium in Lu_2O_3 up to the composition $(Lu_{0.5}Gd_{0.5})_2O_3$, the luminescence time characteristics of the Eu^{3+}-doped scintillating ceramics are very much improved while the density of this latter compound (about 8.4 g/cm^3) is still very favorable. In the first part of the paper the scintillation properties including afterglow measurements of $Lu_2O_3:Eu^{3+}$ and $(Lu_{0.5}Gd_{0.5})_2O_3:Eu^{3+}$ ceramics are investigated. In the second part, the selective excitation of Eu^{3+} in the two cationic sites of the structure unravels reasons for different luminescence decay behaviors and the time reponse improvement of $(Lu_{0.5}Gd_{0.5})_2O_3:Eu^{3+}$ ceramics is discussed.

Experimental Section

The $Lu_2O_3:Eu^{3+}$ and $(Lu_{0.5}Gd_{0.5})_2O_3:Eu^{3+}$ ceramics were elaborated by Saint-Gobain Crystals. The starting powders were synthesized by an inverse coprecipitation method. A solution pH = 10 of ammonia and oxalic acid was prepared. For the synthesis of $Lu_2O_3:Eu^{3+}$, lutetium and europium nitrates were dissolved in ionized water and then added dropwise to the ammonia/oxalic acid solution while stirring. A white precipitate of $Lu_2(C_2O_4)_3:Eu^{3+}$ was formed [17]. The precipitate was washed first with water and then with ethanol before being dried for one hour at 100°C. The powder was then fired at about 800°C. For $(Lu_{0.5}Gd_{0.5})_2O_3:Eu^{3+}$ lutetium, gadolinium and europium nitrates were used. The powders structure was checked by X-ray diffraction and showed pure bixbyite structure with space group Ia-3 (206). Initial Europium concentration was 6 at% and 7 at% (*via* Eu_2O_3) for Lu_2O_3 and $(Lu_{0.5}Gd_{0.5})_2O_3$ ceramics, respectively as this concentration range was found optimum with respect to the light yield of the ceramics [24]. After grinding, pellets were prepared by pressing powders under isostatic conditions at room temperature and then at high temperature. Finally the ceramics were pressed under isostatic conditions at high temperature, before being annealed at 1000°C in air. Both ceramics are 1 cm-diameter large and 1 mm-thick. A Gd_2O_2S:Pr (GOS:Pr) ceramics of 10 mm- diameter and 1 mm-thickness also studied in our laboratory [25] is used as an element of comparison.

Total transmission was measured using a UV-VIS Cary 6000i double beam spectrophotometer. Ceramics samples were placed at the entrance of an integrating sphere. They were excited on their entire surface from the front and light transmitted

and emitted in all directions behind the ceramics was collected by the integrating sphere.

For radioluminescence measurements the ceramics were excited by X-rays produced by a molybdenum tube operated at 50 KV and 20 mA impinging on the samples surface with a 45° angle. Light was collected at 45° angle from the surface *via* an optical fibre by a Princeton Charge Coupled Device (CCD) camera cooled at -65°C coupled with an Acton SpectraPro monochromator.

In thermally stimulated luminescence (TSL) experiments the ceramics were silver glued on a copper sample holder attached to the cold head of a helium closed cycle cryostat. They were first excited for 10 minutes through a beryllium window of the cryostat by a molybdenum X-ray source operated at 50 KV and 20 mA. A Lakeshore temperature controller was then used to apply a 20 K/min heating rate between 10 K and 650 K. Luminescence was collected through a quartz window of the cryostat by the same detection device as the one used in radioluminescence (optical fibre / monochromator / CCD camera).

Afterglow was measured after X-ray excitation provided by a tungsten X-Ray tube operated at 120 kV and 13.3 mA on ceramics placed on a photodiode. Afterglow measurement was carried out with a 1 ms integration time and up to 300 ms.

Laser-excited low temperature luminescence measurements were carried out on ceramics silver glued on a copper sample holder mounted on the cold head of a closed cycle cryogenic refrigerator. The cold head was cooled to 10 K. Fluorescence and decay spectra were recorded using as excitation source an optical parametric oscillator laser (10 Hz, 8 ns) pumped by the third harmonic of a YAG:Nd laser. A Roper/Princeton Intensified Charged Couple Device (ICCD) detector was used to detect the fluorescence with a time delay up to 20 ms.

Results

1. Scintillation properties of $Lu_2O_3:Eu^{3+}$ and $(Lu_{0.5}Gd_{0.5})_2O_3:Eu^{3+}$ ceramics

In-line transmission of $Lu_2O_3:Eu^{3+}$ and $(Lu_{0.5}Gd_{0.5})_2O_3:Eu^{3+}$ ceramics were measured at the main emission wavelength of Eu^{3+}, i.e. 612 nm, as 46 % and 38 %, respectively. Though these values do not appear very high, the ceramics looked transparent. Light was actually very much scattered as samples had not been polished or coated with any anti-reflection layer. As the refractive index of the material is rather high (1.93 and 1.95 at 612 nm for Lu_2O_3 and $(Lu_{0.5}Gd_{0.5})_2O_3$ respectively) a surface treatment is required to avoid light losses. In order to test the ability of the as-prepared ceramics to serve as efficient scintillator pixels used for instance in X-ray CT, their total transmission spectrum was measured and is presented in Figure 1. Let us remind that total transmission was measured with an integrating sphere able to collect both transmitted and scattered light at the back of the ceramics. Therefore total transmission corresponds to light potentially used by a photodetector placed at the back of a scintillating element made of the 1 mm-thick ceramics. Figure 1 shows that $Lu_2O_3:Eu^{3+}$ and $(Lu_{0.5}Gd_{0.5})_2O_3:Eu^{3+}$ ceramics present a total transmission of 81 % and 83 %, respectively at the main emission wavelength of Eu^{3+} (612 nm), indicating that the emitted photons should be efficiently extracted from the materials. Both 1 mm-thick ceramics, prepared here by the same procedure, show a similar and satisfying optical quality in terms of total light transmission.

Note that the transmission spectra of Figure 1 show expected intra-configurational 4f-4f transition lines of Eu^{3+}. The band gaps of Lu_2O_3 and $(Lu_{0.5}Gd_{0.5})_2O_3$ precursor

powders were measured in a previous work as 5.6 eV and 5.4 eV, respectively [24]. These values correspond to the absorption edge observed at the short-wavelength side of the spectra around 220 nm. The spectra also display two absorption bands identified as low transmission dips at 245 nm / 282 nm and at 245 nm / 293 nm for Lu_2O_3:Eu^{3+} and $(Lu_{0.5}Gd_{0.5})_2O_3$:Eu^{3+}, respectively. However this part of the spectrum is modified by the fact that emitted light is not filtered out in this measurement. In that way, the total transmission spectrum at wavelengths where high absorption also reflects some features of an excitation spectrum of Eu^{3+} luminescence. Thus efficient absorption bands for Eu^{3+} luminescence may appear as high transmission values since they imply intense luminescence of Eu^{3+} at 612 nm. Hence the spectrum in that range can alternatively be read as two excitation bands at maxima of the transmission curve, i.e. at 233 nm / 258 nm and 235 nm / 268 nm for Lu_2O_3:Eu^{3+} and $(Lu_{0.5}Gd_{0.5})_2O_3$:Eu^{3+}, respectively. These values are comparable to what was measured by Chen *et al.* on Lu_2O_3:Eu^{3+} ceramics at 245 nm and 266 nm and attributed to charge transfer (CT) absorption bands of Eu^{3+} [26]. Zych *et al.* also observed a double band at 245 nm and 270 nm for a Lu_2O_3 :Eu^{3+} ceramics which they attributed to Eu^{3+} CT bands in the two sites of Lu_2O_3 [27].

The X-ray excited radioluminescence spectra of Lu_2O_3:6%Eu^{3+} and $(Lu_{0.5}Gd_{0.5})_2O_3$:7%Eu^{3+} are shown in Figure 2 along with the radioluminescence spectrum of a standard Gd_2O_2S:Pr^{3+} non-transparent ceramics. The sesquioxides spectra are composed of expected 4f-4f emission lines for Eu^{3+}. The main line corresponds to the $^5D_0 \rightarrow {}^7F_2$ transition of Eu^{3+} at 612 nm and gives a bright red luminescence that perfectly matches silicon photodetectors sensitivity [17]. The other $^5D_J \rightarrow {}^7F_J$ emission lines are identified on the figure and are very similar for both compounds. The integrated intensities for both Lu_2O_3:Eu^{3+} and $(Lu_{0.5}Gd_{0.5})_2O_3$:Eu^{3+}

ceramics are in the range of the intensity for the GOS:Pr ceramics and are similar the one to each other. However no absolute light yield value was here inferred from this comparison as the transparency of the standard and the sesquioxides is different. Pulse-height measurement, which was not available in our laboratory, or comparison with an absolute reference should be carried out in order to measure an absolute light output value. Note that the most recent work indicates a light yield as high as 70 000 photons/MeV obtained with a $(Lu_{0.5}Gd_{0.5})_2O_3$: 10% Eu^{3+} ceramics [28].

Figure 3 shows afterglow measurements of the two ceramics in part per million of the initial light output. At 300 ms $(Lu_{0.5}Gd_{0.5})_2O_3:Eu^{3+}$ ceramics presents an afterglow about one order of magnitude lower than $Lu_2O_3:Eu^{3+}$. Two parts can be distinguished in the decays. Within the first milliseconds (up to 20 ms) the ceramics present a time response in the order of the decay time of Eu^{3+} excited states. Pseudo decay times calculated over the two (τ_1) and three (τ_2) first points are reported in Table 1 as an element of comparison. They are reported here as "short afterglow". Both τ_1 and τ_2 are shorter for $(Lu_{0.5}Gd_{0.5})_2O_3:Eu^{3+}$ than for $Lu_2O_3:Eu^{3+}$. A second part of the afterglow curve can be distinguished between 50 ms and 300 ms. This part of the curves allows us to evaluate the "long afterglow" decay times τ_3 reported in Table 1. The long afterglow decay time is again found shorter for $(Lu_{0.5}Gd_{0.5})_2O_3:Eu^{3+}$ than for $Lu_2O_3:Eu^{3+}$.

TSL glow curves of both ceramics between 10 K and 535 K are shown in Figure 4. The glow curve of $Lu_2O_3:Eu^{3+}$ ceramics presents a main peak at 195 K and two peaks of lower intensity at 54 K and 110 K. The inset of Figure 4 zooms into the 250 K-450 K region. In that region three peaks of much lower intensity can be distinguished at 297 K, 338 K and 375 K. At this point it is difficult to relate with certainty any specific TSL peak to the afterglow observed above. Though of low

intensity, the peaks of the 250 K-450 K region might contribute to the afterglow. However the afterglow at some hundred of ms in $Lu_2O_3:Eu^{3+}$ may most probably be related to the main TSL peak at 195 K. This hypothesis is supported by a study of Kostler *et al.* on $(Y,Gd)_2O_3:Eu^{3+}$ [22] in which the TSL curve of $(Y,Gd)_2O_3:Eu^{3+}$ was found very similar in shape above 150 K to the one presented here for $Lu_2O_3:Eu^{3+}$ with a main peak at 180 K similar to our 195 K peak. By comparing the TSL curve with the afterglow at 100 ms at various temperatures, they showed that the afterglow at 100 ms was unambiguously related to the TSL peak at 180 K.

In Figure 4 the TSL glow curve of $(Lu_{0.5}Gd_{0.5})_2O_3:Eu^{3+}$ presents very similar peaks position to $Lu_2O_3:Eu^{3+}$. The main peak is slightly widened in $(Lu_{0.5}Gd_{0.5})_2O_3:Eu^{3+}$ and its maximum is shifted from 195 K in $Lu_2O_3:Eu^{3+}$ to 205 K. In the 250 K-450 K range, the same low intensity peaks as for $Lu_2O_3:Eu^{3+}$ might be present too though the sensitivity is too low to detect the two last peaks at 338 K and 375 K. Defects responsible for charge trapping in both compounds are therefore probably of same nature. However all peaks of $(Lu_{0.5}Gd_{0.5})_2O_3:Eu^{3+}$ show a strongly reduced intensity compared to those of $Lu_2O_3:Eu^{3+}$.

2. Site selective excitation of Eu^{3+}

A representation of the bixbyite structure of cubic lutetium sesquioxide is shown in Figure 5. It is comparable to fluorine CaF_2 with ¼ anionic vacancy. The oxygen ions constitute a face centered cubic network with oxygen vacancies located on [1 1 1] directions. Two different cationic sites with symmetry C_2 and S_6 exist in a ratio 3:1. C_2 sites are located at the center of the cubes that present two anionic vacancies on a diagonal of a face of the cube. The cations at C_2 occupy 24d Wickoff positions at (u 0

¼). Two oxygen ions are at a medium distance of the C_2 cation (similar to the cation-oxygen distances in S_6 sites), two are at a shorter distance and two at a longer distance. The C_2 cationic site is non centro-symmetric. S_6 sites (or C_{3i}) are located at the center of the cubes that present two anionic vacancies situated on the central diagonal of the cube. The cations occupy 8b Wickoff positions at (¼ ¼ ¼). The six oxygen ions are at equal distance from the central cation. The C_2 cationic site is centro-symmetric. The centro-symmetry character of the site determines the luminescence spectrum of Eu^{3+}.

Up to now contradictory results were published about a possible preferential occupation of Eu^{3+} in one of the two cationic sites of the Lu_2O_3 structure. Concas *et al.* [29] showed that Eu^{3+} occupy mainly C_2 sites in 10%-doped materials whereas a theoretical work from Stanek *et al.* demonstrated that Eu^{3+} should be mainly located at S_6 sites especially at low concentration [30]. Zych *et al.* also confirmed this assertion and furthermore demonstrated that it is impossible to entirely remove 8*b* emission coming from S_6 sites in Lu_2O_3 compounds. However this author indicates that 8*b* emission should be minimized in hosts like Sc_2O_3:Eu^{3+} [31].

As a general LaPorte rule, the 4f-4f dipolar electric transitions of Eu^{3+} are parity forbidden. When Eu^{3+} is located at a centro-symmetric site such as S_6 these transitions remain forbidden. The dipolar magnetic transitions which are anyway much weaker are allowed if $\Delta J = 0, \pm 1$ while $J= 0 \rightarrow J=0$ transitions are forbidden. Hence for Eu^{3+} at the S_6 site at 10 K only $^7F_0 \rightarrow {}^5D_1$ transition in absorption and $^5D_0 \rightarrow {}^7F_1$ transition in emission can be observed. Other $^5D_0 \rightarrow {}^7F_j$ transitions might be observed but with very weak intensity as they originate from vibronic excited states of $^5D_0$. On the contrary, the C_2 site presents no symmetry inversion so that opposite parity states such as 5d are admixed with 4f states. A relaxation of the selection rule therefore takes

place and dipolar electric transitions become partly allowed. Hence for Eu^{3+} in C_2 site all the $^5D_0 \rightarrow {}^7F_j$ transitions can be observed. Those for which $\Delta J = 0, \pm 2$ being "hypersensitive" to this phenomenon are enhanced.

Luminescence spectra of $Lu_2O_3:Eu^{3+}$ and $(Lu_{0.5}Gd_{0.5})_2O_3:Eu^{3+}$ ceramics were recorded at 10 K by exciting the ceramics between 525 nm and 530 nm. This excitation wavelength range allows excitation of Eu^{3+} *via* the $^7F_0 \rightarrow {}^5D_1$ transition which is allowed for Eu^{3+} at both sites. Laser excitation was used in the aim of selectively exciting Eu^{3+} in C_2 or S_6 sites. At 10 K a very limited number of vibronic states of $^5D_0$ are populated. Hence $^5D_0 \rightarrow {}^7F_1$ transitions will be allowed for Eu^{3+} at both sites whereas $^5D_0 \rightarrow {}^7F_0$ transitions will be allowed (forced dipolar electric) for Eu^{3+} in C_2 sites and forbidden for Eu^{3+} in S_6 sites.

The emission spectra of $Lu_2O_3:Eu^{3+}$ for four exciting wavelengths λ_i (i = 1, 2, 3, 4) located between 525 nm and 530 nm with $\lambda_1 > \lambda_2 > \lambda_3 > \lambda_4$ are shown in Figure 6. They display luminescence lines corresponding to intraconfigurational 4f-4f transitions from the excited $^5D_0$ levels of Eu^{3+} to the various spin-orbit split states ^7F_j. The dominant emission line at 611 nm originates from the $^5D_0 \rightarrow {}^7F_2$ hypersensitive transition of Eu^{3+} in C_2. In order to identify the possible contributions of Eu^{3+} at both sites, the shortest wavelength range (580 nm – 605 nm) was looked upon into detail. Two groups of emission lines have been distinguished : (i) a first group (group 1) of lines are present for λ_1 excitation (lowest energy) and their relative intensity decreases when the excitation energy increases (λ_{exc} decreases): they are pointed out on the main graph of Figure 6 at 581.1 nm, 587.5 nm, 593.7 nm and 600-601 nm. (ii) the second group (group 2) of lines are absent for λ_1 excitation and their relative intensity increases when λ_{exc} decreases : they are shown in the insets of Figure 6 at 582.6 nm, 593.1 nm and 596.8 nm. The other emission lines of the 580 nm – 605 nm range are

of lower intensity and are attributed to transitions to various vibronic states of the $^7F_1$ level.

As energy transfer is known to happen from Eu^{3+} in S_6 site to Eu^{3+} in C_2 site [31,32,33] any exciting wavelength λ_i of Figure 6 would allow the observation of the luminescence of Eu^{3+} in C_2 sites either by direct excitation of Eu^{3+} in C_2 or by excitation of Eu^{3+} in S_6 and subsequent energy transfer to Eu^{3+} in C_2. As the lines in group 2 are not observed for λ_1 excitation, group 2 is identified as originating from Eu^{3+} in S_6 whereas group 1 lines are produced by Eu^{3+} in C_2.

For Eu^{3+} in C_2 site the emission line at 581.1 nm being the one at the highest energy is identified as the $^5D_0 \rightarrow {}^7F_0$ transition of Eu^{3+}. The three other emissions at 587.5 nm, 593.7 nm and 600-601 nm were attributed to transitions from $^5D_0$ to the three Stark components of the $^7F_1$ level hence leading to a crystal field splitting of 369 cm^{-1} for the $^7F_1$ level. The energy positions of the $^7F_0$ and the split $^7F_1$ levels named $^7F_{1a}$ $^7F_{1b}$ and $^7F_{1c}$ levels are reported in Table 2. In order to verify this attribution the $^5D_0$ energy position and the barycenter of the $^7F_1$ levels were reported in Figure 7. The figure displays the barycenter law - in that case, for lanthanide cations, only the spin orbit interaction is considered - enounced by Antic-Fidancev [34] corresponding to the position of the $^7F_1$ level barycenter without any effect of the crystal field in regard to the position of the $^5D_0$ level. Data for Eu^{3+} in C_2 lie right on the line of the barycenter law, which corroborates our attribution.

For Eu^{3+} in S_6 site, the attribution of the emission lines shown in the insets of Figure 6 is a little bit more delicate. The emission line at 582.6 nm is very close to the $^5D_0 \rightarrow {}^7F_0$ line of Eu^{3+} in C_2 site (581.1 nm) and one could assume that it would correspond to the $^5D_0 \rightarrow {}^7F_0$ transition of Eu^{3+} in S_6 site as it was reported in Y_2O_3:Eu^{3+} by Hunt and Pappalardo [35]. However this transition is forbidden and

would therefore appear with a somewhat lower intensity. Like several others [32,33] we would rather attribute this line to a $^5D_0 \rightarrow {}^7F_1$ transition. Within this frame two hypotheses can be drawn. In a first hypothesis (hypothesis 1), following Buijs [32], Meijerink and Blasse [16], the lines at 582.6 nm and 593.1 nm would correspond to transitions $^5D_0 \rightarrow {}^7F_{1a}$ and $^5D_0 \rightarrow {}^7F_{1b}$ whereas the line at 596.8 nm would be a transition from $^5D_0$ to a non-fundamental vibronic level of $^7F_1$. According to groups theory the $^7F_1$ levels may split into only two levels, one of them being degenerated. Depending on which one is degenerated two barycenter points (hypothesis 1A and 1B) were calculated as shown in Table 2. Their position is reported in Figure 7. Both points seem too low regarding to the barycenter law of Antic-Fidancev. In a second hypothesis (hypothesis 2), we assume a slightly distorted S_6 site which allows the three $^7F_1$ levels to be non-degenerated. The three lines at 582.6 nm, 593.1 nm and 596.8 nm would then correspond to $^5D_0 \rightarrow {}^7F_{1a}$, $^7F_{1b}$, $^7F_{1c}$ transitions as reported in Table 2. In that case, the barycenter point would be more properly located in Figure 7. We therefore adopted this last hypothesis.

The emission spectra of $(Lu_{0.5}Gd_{0.5})_2O_3:Eu^{3+}$ at 10 K excited at three various wavelengths in the 525 nm – 530 nm range are shown in Figure 8. They present similar features to $Lu_2O_3:Eu^{3+}$ with widened lines. This is explained by the disorder created by the substitution of one half of lutetium ions by larger gadolinium ions. By varying the excitation wavelength the spectra vary less than in the case of $Lu_2O_3:Eu^{3+}$. One can mainly observe the transition lines of $^5D_0 \rightarrow {}^7F_0$ at 581 nm, $^5D_0 \rightarrow {}^7F_1$ (587,7 nm, 593,4 nm and 600,2 nm) of Eu^{3+} in C_2. The energy positions of the levels are reported in Table 2. They are close to values for C_2 site in Lu_2O_3. Note the important fact that for Eu^{3+} in S_6 only the $^5D_0 \rightarrow {}^7F_1$ transition can be observed at 582.2 nm and with a weak intensity. This shows that the occupation ratio of Eu^{3+} in S_6

relative to C_2 is smaller in $(Lu_{0.5}Gd_{0.5})_2O_3:Eu^{3+}$ than in $Lu_2O_3:Eu^{3+}$. This difference between the two compounds will be observed with even more acuity in the following part of the paper (cf. Figure 10).

The decay curves at 10 K of Eu^{3+} in C_2 and S_6 sites was measured by exciting the samples *via* the $^7F_0 \rightarrow {}^5D_0$ line and recording the $^5D_0 \rightarrow {}^7F_{1a}$ emission line. They are shown in Figure 9. The decay profiles of Eu^{3+} in S_6 sites for both sesquioxides were found mono-exponential with a decay time of several milliseconds. For Eu^{3+} in C_2 sites the decays may appear bi-exponential though the second exponential part reaches quickly the background level. Different decay times were calculated depending on the site occupied by Eu^{3+}. In $Lu_2O_3:Eu^{3+}$, the trivalent europium at the S_6 site presents a characteristic lifetime of 4.7 ms whereas its main decay time is 1.4 ms at the C_2 site. These results are in line with decay times found by Zych *et al.* in Lu_2O_3:1%Eu^{3+} at room temperature: 4.4 ms at the S_6 site and 1.4 ms at the C_2 site [31]. In $(Lu_{0.5}Gd_{0.5})_2O_3:Eu^{3+}$, the lifetimes were measured as 3.8 ms and 1.0 ms for Eu^{3+} at the S_6 and C_2 sites, respectively. Hence in both host materials the decay times are much shorter for Eu^{3+} at the C_2 than at the S_6 site, due to the much more symmetrical character of S_6 relative to C_2. On the other hand the $(Lu_{0.5}Gd_{0.5})_2O_3$ host contributes to reducing the decay times of Eu^{3+} in both C_2 and S_6 sites which may be explained by a less symmetrical environment in $(Lu_{0.5}Gd_{0.5})_2O_3$ than in Lu_2O_3. The decay time for the second part of the curves for Eu^{3+} in C_2 sites was not calculated as the signal was too noisy. However the decay time is in the order of some milliseconds. This most probably corresponds to the energy transfer from Eu^{3+} at S_6 sites to Eu^{3+} at C_2 sites as it was shown to take place in ref. 31.

Those different time decaying emissions should therefore contribute to the “short afterglow” of the ceramics as defined in the first paragraph. This can be visualized on

time-resolved luminescence spectra presented in Figure 10. Figure 10.A shows spectra of $Lu_2O_3:Eu^{3+}$. Over the first microseconds (spectrum (a)), emission from Eu^{3+} in C_2 and S_6 sites is observed. The C_2 emission dominates with the hypersensitive $^5D_0 \rightarrow {}^7F_2$ line. Over the 6-9 ms time range one can mainly observe the contribution of Eu^{3+} is S_6 sites as it corresponds to the decay time period of Eu^{3+} in S_6 whereas Eu^{3+} fast emission in C_2 has almost totally vanished. The $^5D_0 \rightarrow {}^7F_2$ hypersensitive transition of Eu^{3+} in C_2 site is also observed with a weak intensity. Over the 20-25 ms time interval the main part of Eu^{3+} emission in both sites has decayed. Only residual emission from both sites is observed with a similar intensity. Similar features are observed in Figure 10 B for $(Lu_{0.5}Gd_{0.5})_2O_3:Eu^{3+}$ with a different ratio between C_2 and S_6 due to different decay times and different repartition of Eu^{3+} ions. Most clearly a main difference between $Lu_2O_3:Eu^{3+}$ and $(Lu_{0.5}Gd_{0.5})_2O_3:Eu^{3+}$ can be underlined in the first microseconds in the zooms of spectra (a) : the intensity of the $^5D_0 \rightarrow {}^7F_0$ line of Eu^{3+} in S_6 is much less important in $(Lu_{0.5}Gd_{0.5})_2O_3:Eu^{3+}$ (B) than in $Lu_2O_3:Eu^{3+}$ (A). Quantitatively the ratio of the emissions from the $^5D_0 \rightarrow {}^7F_0$ line of Eu^{3+} in S_6 over the $^5D_0 \rightarrow {}^7F_{1a}$ line of Eu^{3+} in C_2 varies from 2.2 in $Lu_2O_3:Eu^{3+}$ to 0.4 in $(Lu_{0.5}Gd_{0.5})_2O_3:Eu^{3+}$. This shows again very clearly that the population of S_6 site over C_2 by Eu^{3+} is much lower in $(Lu_{0.5}Gd_{0.5})_2O_3:Eu^{3+}$ than in $Lu_2O_3:Eu^{3+}$.

Discussion

Transparent ceramics of Lu_2O_3: 6% Eu^{3+} and $(Lu_{0.5}Gd_{0.5})_2O_3$: 7 % Eu^{3+} were prepared in a strictly identical way so that the differences between the two samples are limited to the composition. Though it is always difficult to avoid any effect of the

microstructure in a ceramics sample, the two ceramics presented similar total transmission and light output.

By selectively exciting Eu^{3+} at the two cationic sites of the sesquioxide structure we could observe emission of the dopant ion at both sites in the Lu_2O_3:Eu^{3+} and in the $(Lu_{0.5}Gd_{0.5})_2O_3$:Eu^{3+} ceramics though a very different repartition of Eu^{3+} in the two sites was observed according to the composition. The decay time of the emitting excited $^5D_0$ state of Eu^{3+} was found very different from one site to the other. Light emitted from the europium ions located in the non centro-symmetric C_2 site almost totally decayed within $3.\tau_{C2}$, i.e. 4-5 ms in Lu_2O_3:Eu^{3+} and 3-4 ms in $(Lu_{0.5}Gd_{0.5})_2O_3$:Eu^{3+}. Europium ions occupying S_6 sites needed $3.\tau_{S6}$, i.e. 14-15 ms in Lu_2O_3 and 11-12 ms in $(Lu_{0.5}Gd_{0.5})_2O_3$:Eu^{3+} to emit the quasi-totality of their luminescence. Hence the repartition of dopant ions amongst the C_2 and S_6 sites is of great importance as far as the time response of the scintillator is concerned. Even in the hypothesis where no delay is introduced by charge trapping, the sole influence of dopant repartition among the two sites affects what was measured here as the “short afterglow”. Indeed the afterglow measured here up to 20 ms was found more important for Lu_2O_3:Eu^{3+} than for $(Lu_{0.5}Gd_{0.5})_2O_3$:Eu^{3+}. This is directly related with the decay times of Eu^{3+} which were found shorter in $(Lu_{0.5}Gd_{0.5})_2O_3$:Eu^{3+} than in Lu_2O_3:Eu^{3+} at both sites. This can be understood as the presence of gadolinium introduces an asymmetry which may relax the selection rules for 4f-4f transitions and therefore increase the probability in $(Lu_{0.5}Gd_{0.5})_2O_3$:Eu^{3+} of the otherwise forbidden transitions.

Moreover, we showed that the population of S_6 sites by Eu^{3+} is much lower in $(Lu_{0.5}Gd_{0.5})_2O_3$:Eu^{3+} than in Lu_2O_3:Eu^{3+}. As the decay of Eu^{3+} luminescence is at least 3 times longer in S_6 than in C_2 site, this fact will result in a shorter decay of Eu^{3+}

luminescence measured in $(Lu_{0.5}Gd_{0.5})_2O_3:Eu^{3+}$ compared to $Lu_2O_3:Eu^{3+}$. The different Eu^{3+} localization in sites of $(Lu_{0.5}Gd_{0.5})_2O_3:Eu^{3+}$ relative to $Lu_2O_3:Eu^{3+}$ can be understood by considering the sizes of the Lu^{3+}, Gd^{3+} and Eu^{3+} cations. Levy *et al.* [36] showed that in cubic sesquioxides, an isovalent cationic dopant such as Eu^{3+} preferably substitutes the host cation at the C_2 site if it is smaller than the host cation and at the S_6 site otherwise. This would originate from the presence around the cation in C_2 of bonds both shorter and longer than the average distance whereas all the distances are equal in S_6. The shorter bonds in C_2 would therefore favor the presence of smaller cations. In $Lu_2O_3:Eu^{3+}$, Eu^{3+} being larger than Lu^{3+} would preferentially occupy S_6. In $(Lu_{0.5}Gd_{0.5})_2O_3$ the average cationic size is bigger than in Lu_2O_3 so the affinity of Eu^{3+} for S_6 should decrease.

Finally we showed that the "long afterglow" was also higher in $Lu_2O_3:Eu^{3+}$ than in $(Lu_{0.5}Gd_{0.5})_2O_3:Eu^{3+}$. The TSL glow curves were found consistent with this observation as the TSL intensity was highly reduced in $(Lu_{0.5}Gd_{0.5})_2O_3:Eu^{3+}$ compared to $Lu_2O_3:Eu^{3+}$ over the whole temperature range. However we showed that the main TSL peak at around 200 K may be more specifically responsible for afterglow at around 100-300 ms. Trojan *et al.* [20] recently showed that the afterglow in $Lu_2O_3:Eu^{3+}$ was mainly related to Eu^{3+} at S_6 sites. Either the energetic location of Eu^{3+} at S_6 site was more favorable to the transfer from the trap to the luminescent center or the traps were located in the vicinity of Eu^{3+} at S_6 sites [20]. We showed here that $(Lu_{0.5}Gd_{0.5})_2O_3:Eu^{3+}$ favored the location of Eu^{3+} ions more in C_2 sites and less in S_6 sites relative to the host Lu_2O_3. Following the argument of Trojan *et al.*, this would result in less afterglow, and that is precisely what was observed here (see Figure 3).

Alternatively the decrease of TSL intensity may be explained by a reduction in stress and therefore of defects related to Eu^{3+} introduction into the host. One can

briefly analyze the induced distortion of the Lu_2O_3 host when introducing Eu^{3+} as a dopant relatively to distortion occurring in the $(Lu_{0.5}Gd_{0.5})_2O_3$ host. First, one can observe an increase of the measured unit cell parameter from 10.391 Å for Lu_2O_3 to 10.602 Å for $(Lu_{0.5}Gd_{0.5})_2O_3$, in good agreement with the variation of the ionic radii of the constituent (0.95 Å, 0.938 Å and 0.848 Å for Eu^{3+}, Gd^{3+} and Lu^{3+}, respectively). The distortion occurring when introducing Eu^{3+} ions in Lu_2O_3 can be estimated by calculating the ratio of the lattice parameters of Eu_2O_3 (no distortion and a = 10.866 Å) and Lu_2O_3. In this case, the ratio is 4.5%. When introducing Eu^{3+} in the $(Lu_{0.5}Gd_{0.5})_2O_3$ host, the ratio becomes 2.5%. This effect indicates that for $(Lu_{0.5}Gd_{0.5})_2O_3$ compounds the introduction of Eu^{3+} occurs with limited distortions with regard to the Lu_2O_3 host.

Conclusion

We propose a transparent ceramics prepared from the mixed sesquioxide $(Lu_{0.5}Gd_{0.5})_2O_3$ doped with trivalent europium as a potential new scintillator with improved time response characteristics relative to the well-known Lu_2O_3:Eu^{3+}. $(Lu_{0.5}Gd_{0.5})_2O_3$:Eu^{3+} presents a density of about 8.4 g/cm^3, which still lies amongst the highest densities of existing scintillators and therefore is very favorable for efficient X-rays absorption within a small thickness. The measured total transmission was found close to the maximum value (81 %) while no laser quality polishing of the samples has been done (this is usually the case in the scintillator field where the main purpose is to extract the maximum light output).

With afterglow and TSL measurements we demonstrated the advantages of $(Lu_{0.5}Gd_{0.5})_2O_3$:Eu^{3+} ceramics over Lu_2O_3:Eu^{3+}. On the one hand $(Lu_{0.5}Gd_{0.5})_2O_3$:Eu^{3+}

presents a faster intrinsic decay time for Eu^{3+} and on the other hand the ceramics shows a reduced afterglow over the hundreds of milliseconds time range and a reduced TSL intensity over the 10 K - 650 K temperature range.

These improved properties were explained in two terms. First Eu^{3+} intercalation in $(Lu_{0.5}Gd_{0.5})_2O_3:Eu^{3+}$ most probably leads to less distortion than Eu^{3+} in $Lu_2O_3:Eu^{3+}$ as a better cationic size match occurs. Hence less defects in the material may be susceptible to trap charges during irradiation and delay their subsequent transfer and recombination at Eu^{3+} ions. This therefore reducesTSL intensity and afterglow.

Secondly and most of all we demonstrated that $(Lu_{0.5}Gd_{0.5})_2O_3$ composition allows a different repartition of Eu^{3+} ions amongst the C_2 and S_6 cationic sites of the sesquioxide structure. Eu^{3+} ions at both sites in $Lu_2O_3:Eu^{3+}$ and $(Lu_{0.5}Gd_{0.5})_2O_3:Eu^{3+}$ ceramics have been characterized in terms of energy level positions and kinetics of the fluorescence by selectively exciting Eu^{3+} at the two cationic sites of the sesquioxide structure. The $(Lu_{0.5}Gd_{0.5})_2O_3:Eu^{3+}$ compound was shown to greatly favor intercalation of Eu^{3+} in C_2 site over S_6. Eu^{3+} at C_2 site presents a fast decay (1 ms and 1.4 ms for $(Lu_{0.5}Gd_{0.5})_2O_3:Eu^{3+}$ and $Lu_2O_3:Eu^{3+}$), respectively while the decay constant of Eu^{3+} at S_6 site is almost 4 times longer (3.8 ms and 4.7 ms respectively for $(Lu_{0.5}Gd_{0.5})_2O_3:Eu^{3+}$ and $Lu_2O_3:Eu^{3+}$). Thus favoring the substitution by Eu^{3+} at a C_2 site was found to decrease the effective decay time of the ceramics. Additionally the different repartition of Eu^{3+} at C_2 and S_6 sites in the two different ceramics should also have an effect on afterglow as Eu^{3+} at S_6 site may be responsible for afterglow. Further work is now required to determine with more accuracy the light yield and the energy resolution of these promising scintillators.

Acknowledgment

The authors would like to thank Saint-Gobain Crystals and Detectors for their support and especially Northboro Research and Development Center for providing the high quality ceramics and for the afterglow measurements.

1 References

[1] Rossner W, Ostertag M, Jermann F 1999 J Electrochem Soc Proceedings 98 187.

[2] Greskovich CD, Cusano D, Hoffman D, Riedner RJ 1992 Am Ceram Soc Bull 71 1120.

[3] Izumi S, Kamata S, Satoh K 1993 IEEE Trans Nucl Sci 40 158.

[4] Ryzhikov V, Grynyov B, Opolonin A, Naydenov S, Lisetska O, Galkin S, Voronkin E 2007 Rad Measur 42 915.

[5] Weber MJ, Monchamp RR 1973 J Appl Phys 44 5495.

[6] Nestor OH, Huang CY 1975 IEEE Trans Nucl Sci 22 68.

[7] Knoll GF 1999 Radiation Detection and Measurement.

[8] Cooke DW, McClellan KJ, Bennett BL, Roper JM, Whittaker MT, Muenchausen RE, Sze RC 2000 J Appl Phys 88 7360.

[9] Pidol L, Guillot-Noël O, Kahn-Harari A, Viana B, Pelenc D, Gourier D 2006 J. Phys Chem Solids 67 4 643.

[10] Pauwels D, Le Masson N, Viana B, Kahn-Harari A, van Loef EVD, Dorenbos P, van Eijk CWE 2000 IEEE Trans Nucl 47 6 1787.

[11] Pidol L, Kahn-Harari A, Viana B, Ferrand B, Dorenbos P, de Haas JTM, van Eijk CWE, Virey E 2003 J Phys Cond Matter 15 12 2091.

[12] Pidol L, Kahn-Harari A, Viana B, Virey E, Ferrand B, Dorenbos P, de Haas JTM, van Eijk CWE 2004 IEEE Trans Nucl Sci 51 3 1084.

[13] Wang Y, Antonuk L E, Zhao Q, El-Mohri Y, Perna L 2009 Med. Phys. 36 5707.

[14] Valais IG, Michail CM, David SL, Liaparinos PF, Fountos GP, Paschalis TV, Kandarakis IS, Panayiotakis GS 2010 IEEE Trans. Nucl. Sci. 57 3.

[15] Viana B, Bessière A, Rétot H, Mattmann E, LaCourse B. 2011 in press, Opt. Mater., doi:10.1016/j.optmat.2010.10.021.

[16] Blasse G, Grabmaier BC 1994 Luminescent Materials. Springer-Verlag Telos.

[17] Lempicki A, Brecher C, Szupryczynski P, Lingertat H, Nagarkar V, Tipnis S, Miller S 2002 Nucl Instrum Meth Phys.Res A 488 579.

[18] Brecher C, Bartram RH, Lempicki A 2004 J Lumin 106 159.

[19] Kappers L, Bartram R, Hamilton D, Brecher C, Lempicki A 2005 Nucl Instrum Meth Phys Res A 537 443.

[20] Trojan-Piegza J, Zych E 2010 J Phys Chem C 114 4215.

[21] Trojan-Piegza J, Niittykoski J, Hölsä J, Zych E 2008 Chem Mater 20 2252.

[22] Köstler W, Winnaker A, Rossner W, Grabmaier BC 1995 J Phys. Chem Solids 56 907.

[23] Rossner W, Jermann F, Ahne S, Ostertag M 1997 J Lumin 72-74 708.

[24] Rétot H. Phd thesis, 2009, Université Pierre et Marie Curie.

[25] Blahuta S, Viana B, Bessière A, Mattmann E., LaCourse B 2011 Opt. Mater. In press. Doi : 10.1016/j.optmat.2011.02.040

[26] Chen Q, Shi Y, An L, Chen J, Shi J 2006 J Am Ceram Soc 89 2038.

[27] Zych E, Hreniak D, Strek W 2002 J Phys Chem B 106 3805.

[28] Cherepy NJ, Gaume R, Podowitz SR 2010 Oral presentation at symposium on radiation measurements and applications (sorma).

[29] Concas G, Spano G, Zych E, Trojan-Piegza J 2005 J Phys: Condens Matter 17 2597.

[30] Stanek CR, McClellan KJ, Uberuaga BP, Sickafus KE, Levy MR, Grimes RW 2007 Phys Rev B 75 134101.

[31] Zych E, Karbowiak M, Domagala K, Hubert S 2002 J Alloys Compd 341 381.

[32] Buijs M, Meyerink A, Blasse G 1987 J Lumin 37 9.

[33] Garcia-Murillo A. PhD thesis, 2002 Université Claude Bernard Lyon I.

[34] Antic-Fidancev E. 2000 J Alloys Compd 300-301 2.

[35] Hunt RB, Pappalardo RG 1985 J Lumin 34 133.

[36] Levy MR, Stanek CR, Chroneos A, Grimes RW 2007 Solid State Sci 9 588.

1

2

Tables

Table 1 Pseudo-decay times distinguished in the afterglow curves of Lu_2O_3:Eu and $(Lu_{0.5}Gd_{0.5})_2O_3$:Eu ceramics.

	τ_1 (ms)	τ_2 (ms)	τ_3 (ms)
Lu_2O_3:Eu	1.1	3.9	340
$(Lu_{0.5}Gd_{0.5})_2O_3$:Eu	0.9	3.1	210

Table 2 Energy position of Eu^{3+} levels in Lu_2O_3 :Eu and in $(Lu_{0.5}Gd_{0.5})_2O_3$:Eu (in cm^{-1})

Level energy (cm^{-1}) / Site and compound	$^7F_0$	$^7F_{1a}$	$^7F_{1b}$	$^7F_{1c}$	$^7F_1$ barycenter	$^5D_0$
C_2 in Lu_2O_3	0	187	365	556	369	17 208
S_6 in Lu_2O_3 (hyp. 1)	0	139	458	-	245 (hyp. 1A) 352 (hyp. 1B)	17 321 [32]
S_6 in Lu_2O_3 (hyp. 2)	0	139	458	542	380	
C_2 in $(Lu_{0.5}Gd_{0.5})_2O_3$	0	176	349	545	357	17 212

Figure captions

Figure 1. Total transmission spectra of Lu_2O_3 : 6% Eu^{3+} and $(Lu_{0.5}Gd_{0.5})_2O_3$: 7% Eu^{3+} ceramics. Main transitions from the fundamental level $^7F_0$ towards the indicated excited levels of Eu^{3+} are given on the figure.

Figure 2. X-ray excited luminescence spectra of Lu_2O_3 : 6% Eu^{3+} and $(Lu_{0.5}Gd_{0.5})_2O_3$: 7% Eu^{3+} ceramics relative to commercial GOS : Pr^{3+}. The extraction of light between GOS : Pr^{3+} and sesquioxides should not be compared as sesquioxides are transparent whereas GOS :Pr^{3+} is only slightly translucent.

Figure 3. Afterglow curves of Lu_2O_3:Eu and $(Lu_{0.5}Gd_{0.5})_2O_3$:Eu ceramics.

Figure 4. Thermally Stimulated Luminescence (TSL) glow curves of Lu_2O_3 :Eu and $(Lu_{0.5}Gd_{0.5})_2O_3$:Eu ceramics after X-ray irradiation at 10 K. Heating rate : 20 K / minute.

Figure 5. Cristal structure of Lu_2O_3 showing the symmetry of the two cationic sites C_2 and S_6 .

Figure 6. Laser-excited luminescence spectra of Lu_2O_3 : 6% Eu^{3+} excited at four different wavelengths between 525 nm and 530 nm with $\lambda_1 > \lambda_2 > \lambda_3 > \lambda_4$ and recorded at 10 K.

Figure 7. Position of the $^7F_1$ barycenter versus $^5D_0$ level (in red) for Eu^{3+} in the two sites of Lu_2O_3 compared to the barycenter law (in black) from [27]. In blue are drawn the two ruled out hypothesis for position of Eu^{3+} in S_6 site.

Figure 8. Laser-excited luminescence spectra of $(Lu_{0.5}Gd_{0.5})_2O_3$: 7% Eu^{3+} excited at three different wavelengths between 525 nm and 530 nm with $\lambda_1 > \lambda_2 > \lambda_3$ and recorded at 10 K.

Figure 9. Decay profiles of $^5D_0 \rightarrow {}^7F_{1a}$ emission excited at 10K *via* the $^7F_0 \rightarrow {}^5D_0$ transition at 581.2 nm in Lu_2O_3:Eu and 581.3 nm in $(Lu_{0.5}Gd_{0.5})_2O_3$:Eu for Eu^{3+} in C_2 and at 582.6 nm for Lu_2O_3:Eu and 582.9 nm in $(Lu_{0.5}Gd_{0.5})_2O_3$:Eu for Eu^{3+} in S_6. The emission wavelengths are (i) for Lu_2O_3:Eu, 582.7 nm and 587.7 nm for Eu^{3+} in S_6 and C_2 sites, respectively (ii) for $(Lu_{0.5}Gd_{0.5})_2O_3$:Eu, 582.9 nm and 588.1 nm for Eu^{3+} in S_6 and C_2 sites, respectively.

Figure 10. Time-resolved luminescence spectra of Lu_2O_3:Eu (A) and $(Lu_{0.5}Gd_{0.5})_2O_3$:Eu (B) ceramics recorded at 10 K for time intervals indicated on the figure. Ceramics were excited via the $^7F_0 \rightarrow {}^5D_1$ transition at 525 nm- 530 nm.

Figures

Figure 1

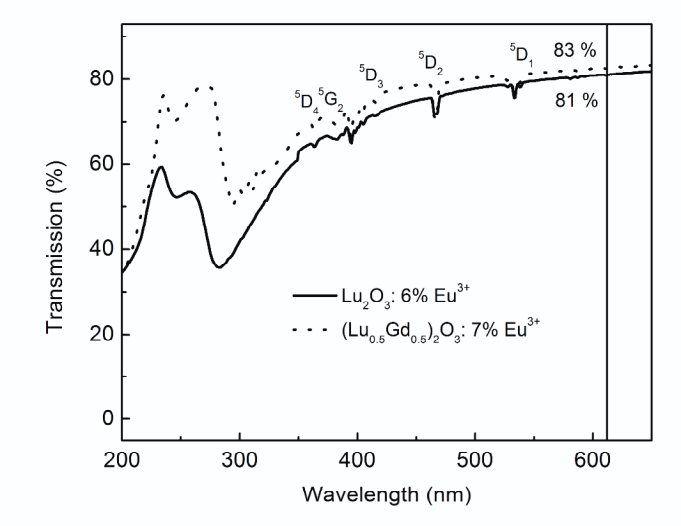

Figure 2

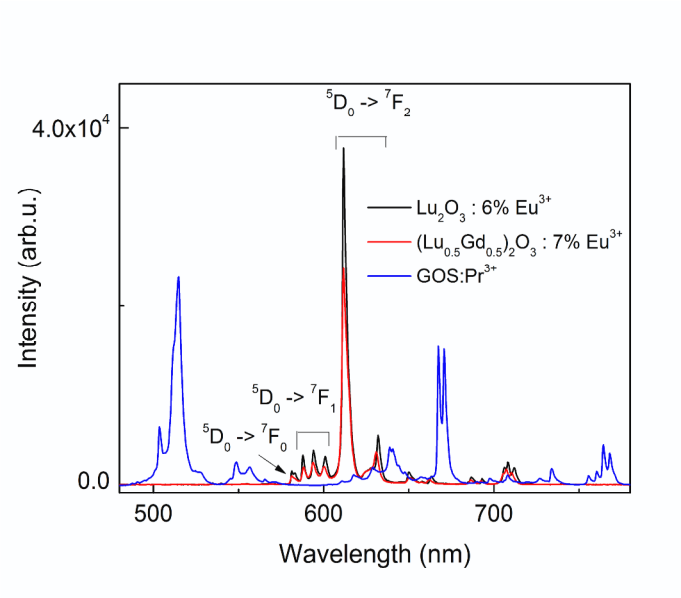

Figure 3

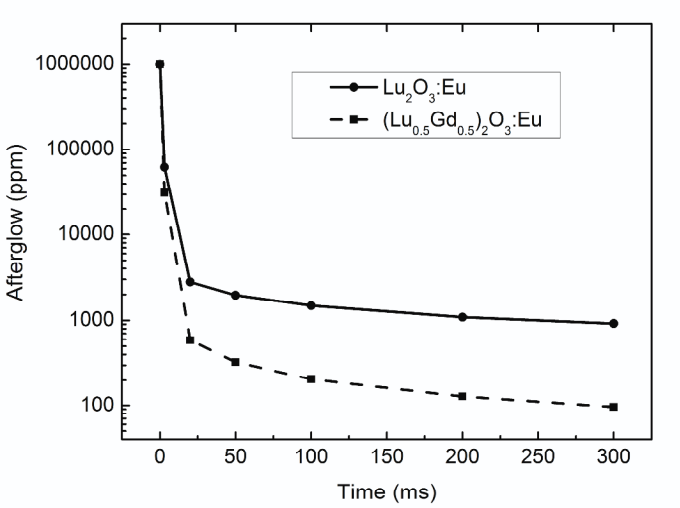

Figure 4

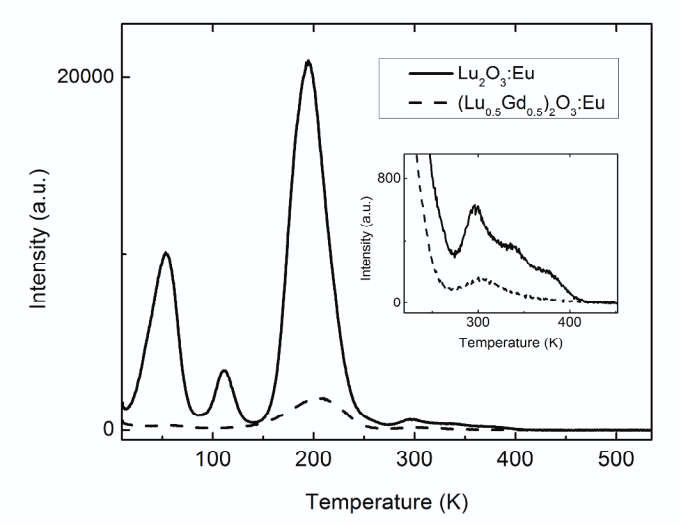

Figure 5

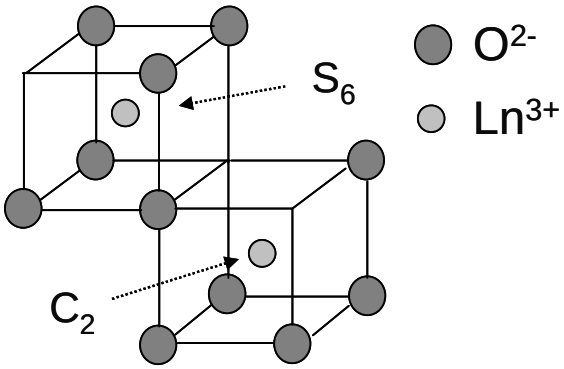

Figure 6

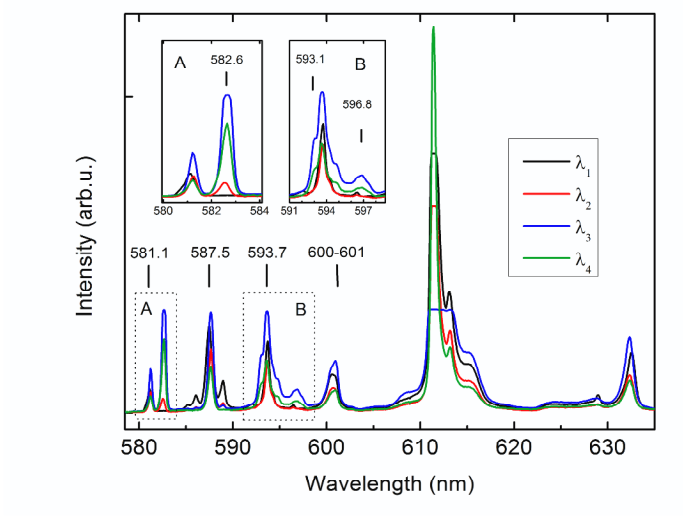

Figure 7

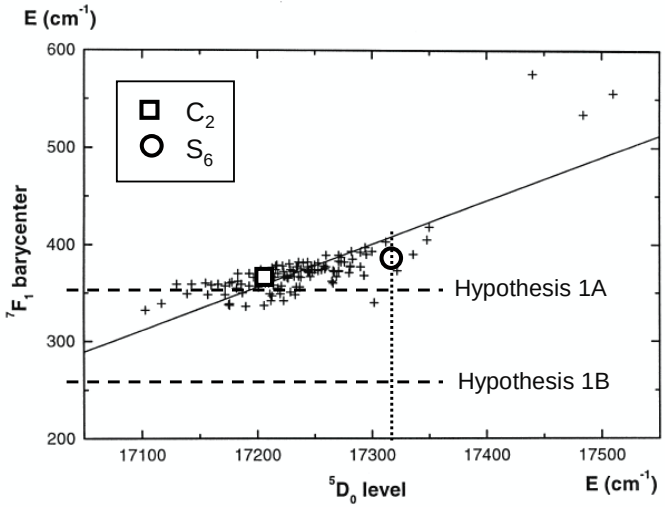

Figure 8

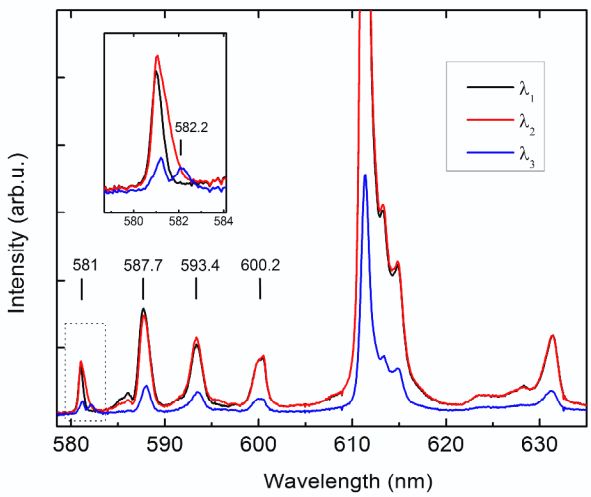

Figure 9

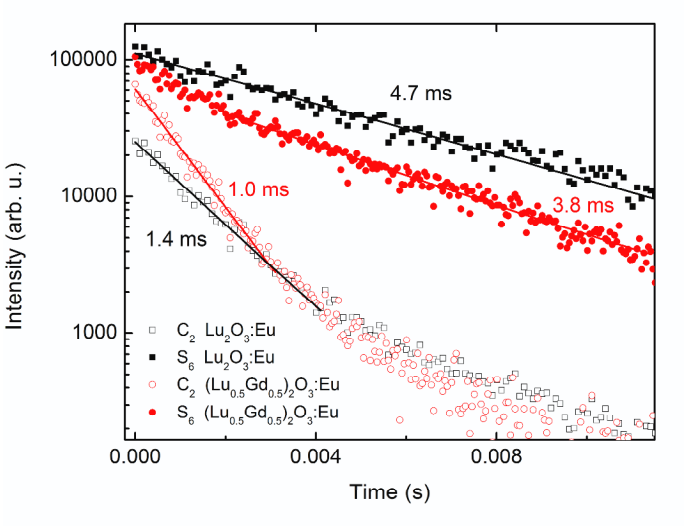
100000
10000
1000
Intensity (arb. u.)
0.000
0.004
0.008
Time (s)
4.7 ms
1.0 ms
3.8 ms
1.4 ms
C2 Lu2O3:Eu
S6 Lu2O3:Eu
C2 (Lu0.5Gd0.5)2O3:Eu
S6 (Lu0.5Gd0.5)2O3:Eu

Figure 10

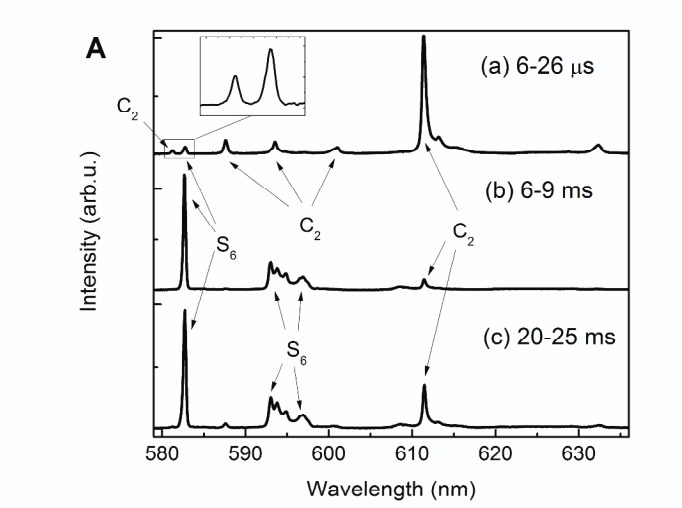
A
(a) 6-26 μs
(b) 6-9 ms
(c) 20-25 ms
C2
C2
C2
S6
S6
Intensity (arb.u.)
580
590
600
610
620
630
Wavelength (nm)

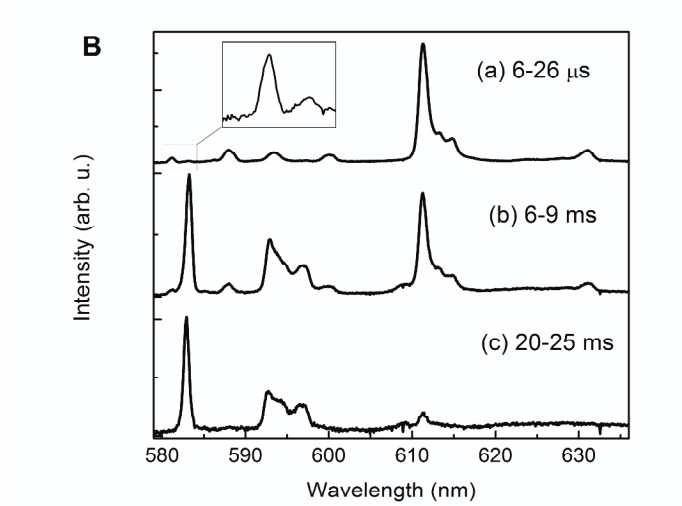
B
(a) 6-26 μs
(b) 6-9 ms
(c) 20-25 ms
Intensity (arb. u.)
580
590
600
610
620
630
Wavelength (nm)